Generating multibreather vector solitons by influencing the Manakov model and its modified forms with the linear self and cross coupling parameters

N. Manikandan [a,*]**, R. Radhakrishnan** [b]

[a] *Mount Zion College of Engineering and Technology, Pudukkottai - 622 507, Tamilnadu, India*

[b] *P.G. and Research Department of Physics, Jamal Mohamed College, Tiruchirappalli - 620 020, Tamilnadu, India*

* Corresponding author.
E-mail address: n.manikandan@mountzion.ac.in (N. Manikandan).

Abstract

We have realized for the first time the multibreather vector multi-solitons supporting collision dynamics with many interaction effects (namely reflection, attraction, beating, etc., effects) associated with the coupled nonlinear Schrödinger family equations having multiple applications. Such effects can be suppressed or enhanced by using the soliton parameters. Here each colliding multibreather vector one-soliton is composed with many soliton and antisoliton parts. Our solutions have freedom to control the number of soliton and antisoliton parts used to compose a vector one-soliton with a definite breathing length. It is also interesting to observe that the breathing maps associated with the obtained solutions depend on their free parameters and also the system parameters. All such investigations help us to realize different breathing mechanisms (namely pedaling, toggling, symmetric compression, symmetric elongation, asymmetric compression, asymmetric elongation, etc.) supported by the colliding one-solitons. An existing breathing mechanism of a given vector breather one-soliton can be suppressed or switched into another mechanism by tuning certain parameters appropriately. Because of such features we believe that this kind of

study will further give impetus on the Lindner–Fedyanin system in the continuum limit, and find the potential applications in fiber coupler and also in Bose–Einstein condensates.

Keywords: Nonlinear physics

1. Introduction

A scalar soliton solution of the nonlinear Schrödinger (NLS) equation propagates with an unchanging profile by exactly compensating the self-phase modulation (SPM) with dispersion (in the case of temporal solitons) or diffraction (in the case of spatial solitons) while in the vector case one must also account for cross-phase modulation (XPM) between components and solve simultaneously a set of coupled nonlinear Schrödinger (CNLS) equations [1, 2, 3]. A shape conserving solution of such equations is known as a vector soliton on account of its multi-component nature. Such solitons can be spatial or temporal in nature. In veracity, such equations are more complicated and not forever integrable. For instance, the straightfoward two component incoherent CNLS equations used to depict the (1+1) dimensional propagation of high intensity pico-second light of arbitrary polarization in the isotropic Kerr media [4, 5]

$$i\frac{\partial q_n}{\partial z} + d\frac{\partial^2 q_n}{\partial x^2} - 2\mu(|q_n|^2 + \sigma|q_{3-n}|^2)q_n = 0, \quad n = 1, 2, \ldots \tag{1}$$

reduce to renowned integrable vector soliton system (namely Manakov model) [6], provided the ratio between nonlinearity thanks to XPM (the coefficient of $|q_{3-n}|^2$) and SPM (the coefficient of $|q_n|^2$) is taken into account to be unity.

In the Eq. (1), q_1 and q_2 are two components of a vector soliton, variables z and x are the longitudinal and transverse co-ordinates respectively, and σ gives the ratio between XPM and SPM values. In the Manakov model, the parameter d can be positive or negative in the temporal case depending on the nature of the dispersion (anomalous or normal). The parameter d takes only positive value in the spatial case which is related to diffraction [1, 2]. Further, the nonlinear parameter μ in (1) may be either negative for the so-called self-focusing (SF) Kerr medium or positive for the self-defocusing (SDF) Kerr medium [3]. Without the loss of generality, one can remove d and μ from the Eq. (1) by properly scaling the components q_1 and q_2 provided $\sigma = 1$. However, here we retain d and μ to conveniently define the existing regions of the different vector soliton forms of the Manakov model.

The scalar one component counterparts of Eq. (1) supports stable localized bright (or dark) soliton [7, 8] if $d\mu < 0$ (or $d\mu > 0$). The bright and dark solitons have completely different nature and they result from the different physical situations corresponding to all four possible sign combinations [9] of μ and d. Because of the

multi-component nature the Manakov case of Eq. (1) admits different forms of the exact two-component vector solitons by coupling two different bright scalar solitons or two different dark scalar solitons or dark and bright scalar solitons [1, 2, 3]. The existing region of the resulting vector soliton solution of the Manakov model depends on the nature of coupling. For example if each scalar component of Eq. (1) in the absence of all the others has $d\mu < 0$ then the Manakov case of Eq. (1) supports (i) the bright–bright (BB) vector soliton with six free real parameters [6, 9, 10], (ii) the bright guided dark (BGD) vector soliton with five free real parameters [11] in the SF Kerr media and (iii) the seven-parameter bright–dark (BD) vector soliton in a parametric domain with the SF nonlinearity [12] as solutions. Similarly if q_1 and q_2 are scalar components with $d\mu > 0$ then the Manakov model which couples such components admits (i) the dark–dark (DD) vector soliton with eight free real parameters [13], (ii) the five-parameter dark guided bright (DGB) vector soliton [11] in the SDF Kerr media and (iii) the seven-parameter BD vector soliton in a parametric domain with the self-defocusing nonlinearity [12] as solutions. Among which the BB vector solitons exhibit energy exchange collision among the components of colliding solitons in the SF Kerr media [14, 15]. This cascaded collision dynamics of BB vector soliton lays experimental foundation for optical computation [16, 17, 18] and information transfer [19]. Anastassiou et al. [20] observed such strongly exchange collision experimentally. Moreover it was investigated in diverse areas [21, 22, 23, 24, 25] including Bose–Einstein condensates [23], X-junction multi-port devices [21], lattice based quantum representation [24], etc. Very recently such nature of collision has also been numerically demonstrated in the SDF region [26]. This study may also lead to many practical applications as in the SF case.

Although the Manakov model does not couple one component with $d\mu > 0$ and other component with $d\mu < 0$, the modified Manakov soliton system with such mixed nonlinearities can be realized from the Eq. (1) provided $\sigma = -1$ [27, 28, 29, 30, 31, 32]. It is also interesting to note that eventhough both the parameters d and μ in any one of the components of this modified Manakov equation change their signs simultaneously then the resulting equation with the mixed nonlinearities also has the Painlevé's (P) integrability property [29]. In the modified Manakov case, one can directly realize the dark–dark [10], the bright–bright [33, 34], and the bright–dark [35, 36, 37] vector soliton solutions by making trivial changes in the corresponding manipulations made for the Manakov case by using the Hirota's technique. The possible physical realizations of such modified Manakov model arise in the contexts of Boson–Fermion gas mixtures [38, 39], BECs involving two isotopes of the same element [40], multi-field propagation in a quadratic medium with inefficient phase matching [41] and Bose–Hubbad model [42]. Moreover Lazarides and Tsironis [22] have used the Eq. (1) as a mathematical model to govern the electromagnetic pulse propagation in the isotropic and homogeneous nonlinear left handed material.

In this paper we have analyzed the behavioral changes in the five-parameter BGD and DGB vector soliton solutions of the Manakov model [11] by changing the signs of d, μ, and σ. Particularly, section 2 is conveniently used to show that both the BGD and DGB vector soliton solutions of the Manakov model become a five-parameter BD vector soliton by making a simple modification in their mathematical expressions while the cross-phase modulation (XPM) coefficient of the Manakov model alters its sign. Further this BD vector soliton solution and other possible solutions of the modified equation with mixed nonlinearities obtained by simultaneously changing the signs of SPM and dispersion coefficients of any one of its scalar component can be directly derived through the simple transformations realized by comparing the Hirota bilinear forms of the Manakov model and its modified form as shown in the section 2. Section 3 reveals that all such solutions modify their nature as multibreather vector one-solitons with different breathing maps, if the linear coupling terms are added suitably in the respective Manakov model and its modified form without loss of their integrability properties in accordance with many earlier studies [42, 43, 44, 45, 46, 47, 48, 49, 50]. Moreover the number of soliton and anti-soliton parts composed in each breather with a definite breathing length can be controlled by tuning its free parameters for pulse-width, velocity, and depth of localization appropriately. Section 3.3 is used to study the nature of collision between two different multibreather vector one-solitons by constructing a multibreather vector multi-soliton solution. Our solution supports different collision scenarios. Specifically we have noted reflection, attraction, and beating effects in the collision regions of different pairs of colliding breather vector one-solitons. Our solution has freedom to control the nature of collision effect and the nature of breathing mechanism associated with the colliding breather vector one-solitons. Finally, section 4 is reserved for conclusion.

2. Theory/calculation

By using the Hirota bilinear transformations $q_1 = g/f$ and $q_2 = h/f$ (where $g(z, x)$ and $h(z, x)$ are complex functions and $f(z, x)$ is a real function), Eq. (1) can be rewritten while $\sigma = +1$ as

$$f[(iD_z + dD_x^2 - \lambda)g \cdot f] - g[(dD_x^2 - \lambda)f \cdot f + 2\mu(gg^* + hh^*)] = 0,$$
$$f[(iD_z + dD_x^2 - \lambda)h \cdot f] - h[(dD_x^2 - \lambda)f \cdot f + 2\mu(gg^* + hh^*)] = 0, \qquad (2)$$

where

$$D_z^m D_x^n g(z, x) \cdot f(z, x) = \left(\frac{\partial}{\partial z} - \frac{\partial}{\partial z'}\right)^m \left(\frac{\partial}{\partial x} - \frac{\partial}{\partial x'}\right)^n g(z, x) \cdot f(z', x')|_{z=z', x=x'}.$$

The above Eq. (2) can be decoupled as the following set of bilinear equations

$$(iD_z + dD_x^2 - \lambda)g \cdot f = 0, \quad (iD_z + dD_x^2 - \lambda)h \cdot f = 0,$$
$$(dD_x^2 - \lambda)f \cdot f = -2\mu(gg^* + hh^*), \qquad (3)$$

where $*$ denotes the complex conjugate and λ is an unknown decoupling constant to be determined. By following the algorithmic steps of Hirota's method as in the Ref. [11], one can derive the five-parameter vector one-soliton solution with the help of Eq. (3) as

$$q_{1M} = \tau e^{i(\psi_1 + \varphi + \pi)}[i\sin\varphi + \cos\varphi \tan h(\eta_{1R} + \frac{\xi}{2})],$$

$$q_{2M} = \sqrt{|\tau|^2 \cos^2\varphi - \frac{d}{\mu}k_{1R}^2}(e^{i\eta_{1I}})\sec h(\eta_{1R} + \frac{\xi}{2}), \qquad (4)$$

where $\psi_1 = lx - (dl^2 + \lambda)z + \psi_1^{(0)}$, $\cos\varphi = k_{1R}/\sqrt{|p_1|^2}$, $\sin\varphi = (k_{1I} - l)/\sqrt{|p_1|^2}$, $\eta_{1R} = k_{1R}x - 2dk_{1R}k_{1I}z + \eta_{1R}^{(0)}$, $\eta_{1I} = k_{1I}x + [d(k_{1R}^2 - k_{1I}^2) - \lambda]z + \eta_{1I}^{(0)}$, $\lambda = 2\mu|\tau|^2$, $\xi = ln\left(\frac{4|\tau|^2 k_{1R}^2}{|p_1|^2} - \frac{4dk_{1R}^2}{\mu}\right)^{-1}$ and $|p_1|^2 = k_{1R}^2 + (k_{1I} - l)^2$. There are five free real parameters namely k_{1R}, k_{1I}, l, τ_R, and τ_I in the above solution. These can be characterized as explained below. The envelope phase $(\eta_{1R} + \frac{\xi}{2})$ of Eq. (4) reveals that k_{1R} and k_{1I} represent the envelope width and envelope speed of both the components. Next to understand the role of l, the changes in q_{1M} of Eq. (4) while φ varies as a function of k_{1R}, k_{1I}, and l should be examined. It is interesting to note that with respect to the value of φ, the vector soliton (4) can be classified into (i) DB vector soliton with fundamental dark component under the condition $k_{1I} = l$ (i.e., at $\varphi = 0$), (ii) DB vector soliton with gray dark component under the condition $k_{1I} \neq l$ (i.e., $\varphi \neq 0$). That is, if $\varphi = 0$, q_{1M} component has no intensity at $\eta_{1R} + \frac{\xi}{2} = 0$ and becomes as the fundamental dark soliton. In the $\varphi \neq 0$ case, the minimum intensity of q_{1M} can be varied by tuning φ with the help of k_{1R}, k_{1I}, and l.

From the expression for ξ in the Eq. (4), it is obvious that the Eq. (4) is as such valid if $d\mu < 0$. However in the case of $d\mu > 0$, the Eq. (4) is valid provided $\frac{|\tau|^2}{|p_1|^2} > \frac{d}{\mu}$. Therefore the physical nature of each case is different. For example, if $d\mu > 0$ then the bright component of Eq. (4) does not exist without the support of dark component due to the restriction $\frac{|\tau|^2}{|p_1|^2} > \frac{d}{\mu}$. Therefore such case is referred as dark guided bright (DGB). Similarly for $d\mu < 0$, the dark component does not exist alone. In this case Eq. (4) is as such called as the bright guided dark (BGD) vector soliton.

For $\sigma = -1$, the Eq. (1) can be read as

$$i\frac{\partial q_n}{\partial z} + d\frac{\partial^2 q_n}{\partial x^2} - 2\mu(|q_n|^2 - |q_{3-n}|^2)q_n = 0, \quad (n = 1, 2, ...) \qquad (5)$$

By using the Hirota bilinear transformations as in $\sigma = +1$ case, Eq. (5) can be rewritten as

$$f[(iD_z + dD_x^2 - \lambda)g \cdot f] - g[(dD_x^2 - \lambda)f \cdot f + 2\mu(gg^* - hh^*)] = 0,$$

$$f[(iD_z + dD_x^2 - \lambda)h \cdot f] - h[(dD_x^2 - \lambda)f \cdot f + 2\mu(gg^* - hh^*)] = 0. \qquad (6)$$

The above Eq. (6) can be decoupled as

$$(iD_z + dD_x^2 - \lambda)g \cdot f = 0, \quad (iD_z + dD_x^2 - \lambda)h \cdot f = 0,$$
$$(dD_x^2 - \lambda)f \cdot f = -2\mu(gg^* - hh^*). \tag{7}$$

By comparing the bilinear equations (3) and (7) of the $\sigma = +1$ case and the $\sigma = -1$ case, one can note that there is a change of sign in the last term of last equation. Therefore by exploiting the systematic procedure of the Hirota method, we have directly realized the mixed vector soliton solution of the modified Manakov model by interchanging the two terms within the square root of the amplitude part of q_{2M} and also making a similar change in the ξ term of the Eq. (4). That is the amplitude part and the term ξ of the modified Manakov model become respectively as $\sqrt{\dfrac{dk_{1R}^2}{\mu} - |\tau|^2 \cos^2 \varphi}$ and $\ln\left(\dfrac{4dk_{1R}^2}{\mu} - \dfrac{4|\tau|^2 k_{1R}^2}{|p_1|^2}\right)^{-1}$ without disturbing other parts of Eq. (4).

Eventhough such changes are trivial, we have noted that the mixed vector soliton solution of the modified Manakov model is valid only in the region $d\mu > 0$ provided $\dfrac{d}{\mu} > \dfrac{|\tau|^2}{|p_1|^2}$. But in the Manakov case such solution is valid for both the $d\mu > 0$ and $d\mu < 0$ cases as mentioned before. Moreover the mixed vector soliton solution of the modified Manakov model is helpful to realize a fact that both the q_1 and q_2 components exist in the absence of other. It is interesting to note that here q_1 exists in the SDF region while q_2 is absent or q_2 exists in the SF region while q_1 is absent. Therefore we have named the five-parameter mixed vector soliton solution of the modified Manakov model as the five-parameter BD vector soliton solution in the SDF region. In this modified Manakov model (i.e., $\sigma = -1$ case), if we change the signs of d and μ simultaneously in any one of the component then the resultant equation couples two components with different nonlinearities and preserves its P-property [29]. For example, one can make such change in the q_1 component then the resultant solution can be read from the solution of the actual case through the transformation $q_2 \to q_2^*$ and $k_{1I} = -k_{1I}$. For the other similar possible change the transformation equations are $q_1 \to q_1^*$ and $l = -l$.

3. Results and discussion

By including the linear coupling terms in the Eq. (1) considerable attentions were paid on the resultant coupled soliton equations [42, 43, 44, 45, 46, 47, 48, 49, 50]. Such equations model the Lindner–Fedyanin system [28, 42, 51] which is a 1D continuum limit of 2D Hubbard model. Further the Eq. (1) with the linear coupling terms has been realized recently as a mathematical model for the experimentally designed structural rocking filter made by using the highly birefringent photonic crystal fiber [47]. Another physical model associated with such equation is two-component BECs, where the signs of SPM and XPM coefficients can be tuned suitably through Feshbach resonance [48]. In the case of nonlinear coupler the numerical value of σ in the Eq. (1) with the linear coupling terms depends on the

overlap between the q_1 and q_2 modes [48]. For example the dual-core coupler has relatively small σ value. The performance of nonlinear single-core coupler or rocking rotator can also be studied by using such equation with relatively large σ value [48, 52, 53]. At this point it is worth to point out that considerable attentions were focused to study the effects of linear coupling terms on the Manakov model and its modified forms [44, 45, 46, 47, 49]. In this section, to the best of our knowledge, we have derived the exact multibreather vector solitons with different breathing maps by solving such equations for the first time. The breathing maps associated with the different initial intensity profiles were also characterized.

3.1. Multibreather vector soliton solutions of the Manakov model with linear coupling parameters

By adding the linear coupling terms in the Eq. (1), then the Manakov model ($\sigma = +1$) can be rewritten [44, 45, 46, 47, 49] as

$$iq_{1_z} + dq_{1_{xx}} + \rho q_1 + \kappa q_2 - 2\mu(|q_1|^2 + |q_2|^2)q_1 = 0,$$
$$iq_{2_z} + dq_{2_{xx}} - \rho q_2 + \kappa q_1 - 2\mu(|q_1|^2 + |q_2|^2)q_2 = 0, \tag{8}$$

where ρ is the linear self-coupling coefficient and κ is the cross-coupling coefficient. Using the following transformation [45]

$$q_1 = \cos(\theta/2)e^{i\Gamma z}q_{1M} - \sin(\theta/2)e^{-i\Gamma z}q_{2M},$$
$$q_2 = \sin(\theta/2)e^{i\Gamma z}q_{1M} + \cos(\theta/2)e^{-i\Gamma z}q_{2M}, \tag{9}$$

where $\Gamma = \sqrt{\rho^2 + \kappa^2}$ and $\theta = \tan^{-1}(\kappa/\rho)$, the Eq. (8) can be related to the Manakov model. For coupled system, both the linear coupling constants κ and ρ are present, then the Eq. (8) has an periodic intensity exchange between the orthogonally polarized modes [45]. When the linear self-coupling coefficient is absent (i.e., $\rho = 0$), then the Eq. (8) has a simple solitary wave solution exhibiting energy switching between the modes [44]. If both the linear coupling constants are absent (i.e., $\kappa = \rho = 0$) then one can easily recognize the system (8) to be celebrated as an integrable Manakov model (1). Thereby substituting the mixed vector one-soliton solution (4) of the Manakov model in (9) one can read the one-soliton solution of (8) as

$$q_1 = -\cos(\theta/2)\tau e^{i(\psi_1+\varphi+\Gamma z)}\left[i\sin\varphi + \cos\varphi\tan h(\eta_{1R} + \frac{\xi}{2})\right]$$
$$-\sin(\theta/2)\sqrt{|\tau|^2\cos^2\varphi - \frac{d}{\mu}k_{1R}^2}\quad(e^{i(\eta_{1I}-\Gamma z)})\ \sec h(\eta_{1R} + \frac{\xi}{2}),$$
$$q_2 = -\sin(\theta/2)\tau e^{i(\psi_1+\varphi+\Gamma z)}\left[i\sin\varphi + \cos\varphi\tan h(\eta_{1R} + \frac{\xi}{2})\right]$$
$$+\cos(\theta/2)\sqrt{|\tau|^2\cos^2\varphi - \frac{d}{\mu}k_{1R}^2}\quad(e^{i(\eta_{1I}-\Gamma z)})\ \sec h(\eta_{1R} + \frac{\xi}{2}). \tag{10}$$

To facilitate the understanding of the dynamical behavior with reference to the periodic intensity variation of q_1 and q_2, it is convenient to obtain $|q_1|^2$ and $|q_2|^2$ from (10) as

$$|q_1|^2 = \cos^2(\theta/2)|\tau|^2 \sin^2\varphi + \cos^2(\theta/2)|\tau|^2 \cos^2\varphi \tanh^2(\eta_{1R} + \frac{\xi}{2}) + \sin^2(\theta/2)$$

$$(|\tau|^2\cos^2\varphi - \frac{d}{\mu}k_{1R}^2)\sec h^2(\eta_{1R} + \frac{\xi}{2}) - \sin\theta|\tau|\sqrt{|\tau|^2\cos^2\varphi - \frac{d}{\mu}k_{1R}^2}$$

$$\sec h(\eta_{1R} + \frac{\xi}{2})\sin\varphi \sin(\psi_1 + \varphi + \zeta - \eta_{1I} + 2\Gamma z)$$

$$+ \sin\theta|\tau|\sqrt{|\tau|^2\cos^2\varphi - \frac{d}{\mu}k_{1R}^2}\sec h(\eta_{1R} + \frac{\xi}{2})\cos\varphi \tanh(\eta_{1R} + \frac{\xi}{2})$$

$$\cos(\psi_1 + \varphi + \zeta - \eta_{1I} + 2\Gamma z),$$

$$|q_2|^2 = \sin^2(\theta/2)|\tau|^2 \sin^2\varphi + \sin^2(\theta/2)|\tau|^2 \cos^2\varphi \tanh^2(\eta_{1R} + \frac{\xi}{2}) + \cos^2(\theta/2)$$

$$(|\tau|^2\cos^2\varphi - \frac{d}{\mu}k_{1R}^2)\sec h^2(\eta_{1R} + \frac{\xi}{2}) + \sin\theta|\tau|\sqrt{|\tau|^2\cos^2\varphi - \frac{d}{\mu}k_{1R}^2}$$

$$\sec h(\eta_{1R} + \frac{\xi}{2})\sin\varphi \sin(\psi_1 + \varphi + \zeta - \eta_{1I} + 2\Gamma z)$$

$$- \sin\theta|\tau|\sqrt{|\tau|^2\cos^2\varphi - \frac{d}{\mu}k_{1R}^2}\sec h(\eta_{1R} + \frac{\xi}{2})\cos\varphi \tanh(\eta_{1R} + \frac{\xi}{2})$$

$$\cos(\psi_1 + \varphi + \zeta - \eta_{1I} + 2\Gamma z), \tag{11}$$

where $\tau = |\tau|e^{i\zeta}$.

From the above equations (10), (11) it is obvious to note that if the effect of linear cross-coupling (κ) is absent (i.e., $\theta = 0°$) in the presence of linear self-coupling (ρ) then the components q_j become $q_j = q_{j_M}e^{\mp(-1)^j * i\rho * z}$, $j = 1, 2, ...n$. Since here ρ appears only in the z coefficient of the complex modulation of each component, the intensity profiles of the two components of the vector soliton (11) do not differ from those of the mixed vector soliton equation (4). If we increase θ value in order to introduce the effect of κ then some changes appear in the intensity profiles of the $\theta = 0°$ (i.e., $\kappa = 0$, $\rho \neq 0$) case. As an example for some special values of θ, namely $\theta = 45°$ where $\kappa = \rho$ and $\theta = 90°$ where $\rho = 0$, $\kappa \neq 0$, we have numerically demonstrated such changes in the form of periodically varying breather vector solitons with different breathing maps as shown in Figures 1, 2, 3, 4, 5, 6 and 7 not only by tuning the five free parameters but also changing the signs of SPM and XPM coefficients.

In order to have convenient discussion, now we simplify the expression (11) by exploiting the condition $l = k_{1I}$ (or $\varphi = 0$) used to create the fundamental dark and bright components in the vector one-soliton (4) as

$$|q_1|^2 = \left[\cos(\theta/2)|\tau|\tanh(\eta_{1R} + \frac{\xi}{2}) + \sin(\theta/2)\sqrt{|\tau|^2 - \frac{d}{\mu}k_{1R}^2}\sec h(\eta_{1R} + \frac{\xi}{2})\right]^2$$

$$- \sin(\theta)|\tau|\sqrt{|\tau|^2 - \frac{d}{\mu}k_{1R}^2} \tanh(\eta_{1R} + \frac{\xi}{2}) \sec h(\eta_{1R} + \frac{\xi}{2})$$

$$[1 - \cos(\psi_1 + \zeta - \eta_{1I} + 2\Gamma z)],$$

$$|q_2|^2 = \left[\sin(\theta/2)|\tau| \tanh(\eta_{1R} + \frac{\xi}{2}) + \cos(\theta/2)\sqrt{|\tau|^2 - \frac{d}{\mu}k_{1R}^2} \sec h(\eta_{1R} + \frac{\xi}{2}) \right]^2$$

$$- \sin(\theta)|\tau|\sqrt{|\tau|^2 - \frac{d}{\mu}k_{1R}^2} \tanh(\eta_{1R} + \frac{\xi}{2}) \sec h(\eta_{1R} + \frac{\xi}{2})$$

$$[1 + \cos(\psi_1 + \zeta - \eta_{1I} + 2\Gamma z)]. \tag{12}$$

The first two terms of Eq. (11) define gray-dark (GD) and bright intensity profiles while in the case of Eq. (12) the first two terms represent fundamental dark (FD) and bright intensity profiles. In the case of Eq. (11) $\varphi \neq 0$. Therefore it contains the last two terms with the periodic functions of z and x. But due to the restriction $l = k_{1I}$ (i.e., $\varphi = 0$), the Eq. (12) has an oscillating term. The two analytical expressions (11) and (12) are very helpful to interpret the influence of such oscillating terms through their numerical plots obtained for different parametric choices in the following part of discussion. The oscillating terms in the equations (11) and (12) reveal that there is a periodic change in the intensity profiles of the components q_j, $j = 1, 2...$ provided both $\kappa \neq 0$ and $|\tau|^2 \cos^2\varphi \neq \frac{d}{\mu}k_{1R}^2$. Such periodic variation associated with the Eq. (11) and the Eq. (12) can be defined by using their phase of the oscillating terms respectively as

$$L_{cg} = \frac{2\pi}{(dk_{1I}^2 - dl^2 - dk_{1R}^2 + 2\sqrt{\rho^2 + \kappa^2})}, \tag{13}$$

and

$$L_{cf} = \frac{2\pi}{(-dk_{1R}^2 + 2\sqrt{\rho^2 + \kappa^2})}. \tag{14}$$

As one expects the Eq. (14) follows from the Eq. (13) under the condition $l = k_{1I}$. These equations define the length at which the initial profiles of (11) and (12) (i.e., $|q_1|^2$ and $|q_2|^2$ at $z = 0$) appear periodically during the propagation along the z-axis.

As mentioned before in the absence of coupling coefficient κ there is no such periodic variation. Therefore first we want to analyze such periodic variation in the coupling length L_{cf} and then in the coupling length L_{cg} systematically by tuning θ with the help of κ. We are performing such studies by selecting different possible parametric values without violating the condition $|\tau|^2 \cos^2\varphi \neq \frac{d}{\mu}k_{1R}^2$. The value of θ (i.e., the role of ρ and κ) defines the amount of contribution of the first two terms in the Eqs. (11), (12) and the influence of oscillating terms. For example the first two terms equally contribute only if $\theta = n\pi/2$ ($\kappa \neq 0$, $\rho = 0$), ($n = 1, 3, 5, ..$). Under the given parametric values the oscillating terms give their maximum contribution as for as this θ value is concerned. For $\theta = n\pi$ or $\kappa = 0$, $\rho \neq 0$ ($n = 0, 2, 4..$), $|q_1|^2$ and $|q_2|^2$ are the intensity profiles of FD and bright without any oscillations. However if
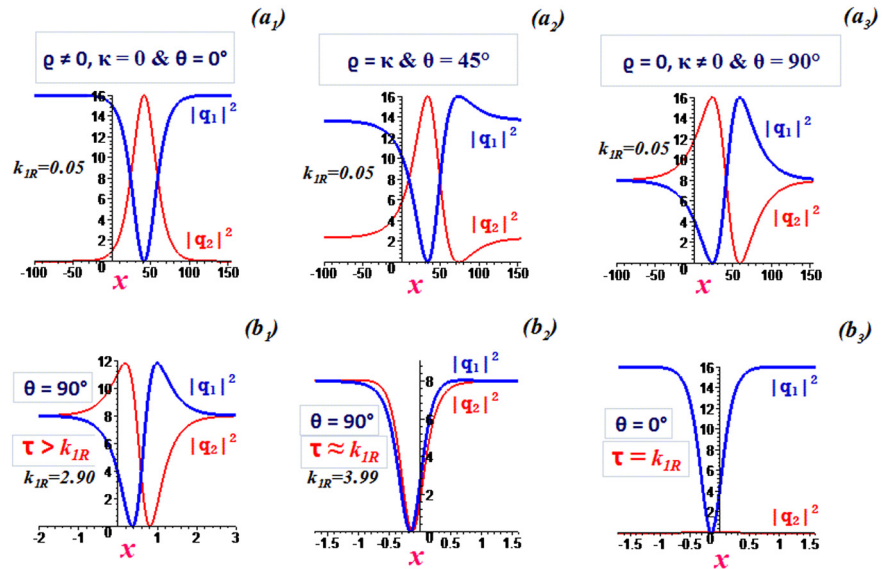
Figure 1. (a_1-a_3) An initial profile of Eq. (12) for a given θ value (i.e., with a particular breathing still) can be switched into another breathing still form. By tuning k_{1R} value in the (a_3) as shown in (b_1) $k_{1R} =$ 2.90, (b_2) $k_{1R} = 3.99$ FD–FD form (if $d\mu > 0$) and (b_3). Note that the amplified scalar D-soliton appears (if $\theta = 0°$, $\tau = k_{1R}$, and $d\mu > 0$).

$n = 1, 3, 5..$, such intensity profiles switch their forms from one component to other. Moreover in this paper we have shown that due to the different nature of Eq. (11) and Eq. (12), the Eq. (11) supports multibreather vector soliton solutions composed with many soliton and antisoliton parts while the Eq. (12) supports breather solitons composed with a pair of soliton and antisoliton. The nature of breathing mechanism of each case not only depends on the five solution free parameters but also depends on the system parameters θ, d, μ and σ. In this paper by considering the suitable parametric values the breathing maps within the range $\theta = 0°$ to $90°$ are analyzed. Such studies can be related to the results associated with the other θ values through some symmetric transformations. Moreover the role of free parameters in each θ case is analyzed systematically as shown below.

Figure 1(a_1) shows an intensity profile of the Eq. (12) at $z = 0$ under the parametric values $\tau = 4.0$, $k_{1R} = 0.05$, $k_{1I} = l = 0.25$, $\kappa = 0.0$, $\rho = 0.25$ and $d = \mu = 0.5$. In this profile q_1 supports fundamental dark (FD) component while q_2 supports bright component although linear self-coupling effect (ρ) exists in the absence of cross-coupling effect (κ) (i.e., $\theta = 0°$). The nature of this initial profile takes different forms as shown in the Figure 1, if we gradually introduce the effect of κ by tuning θ. The initial profiles with $\theta \neq 0$ vary periodically and form moving breather vector solitons as shown in Figure 2 with different breathing maps as shown in Figure 3 provided $\tau \neq k_{1R}$. The numerical values for L_{cf} realized from the Figures 2, 3 agree with the Eq. (14). In the cases (i) $\theta \neq 0$ and $\tau = k_{1R}$, (ii) $\theta = 0°$ and $\tau = k_{1R}$, and (iii) $\theta = 0°$ but $\tau \neq k_{1R}$, with $d\mu > 0$, the breathing effects disappear by forming
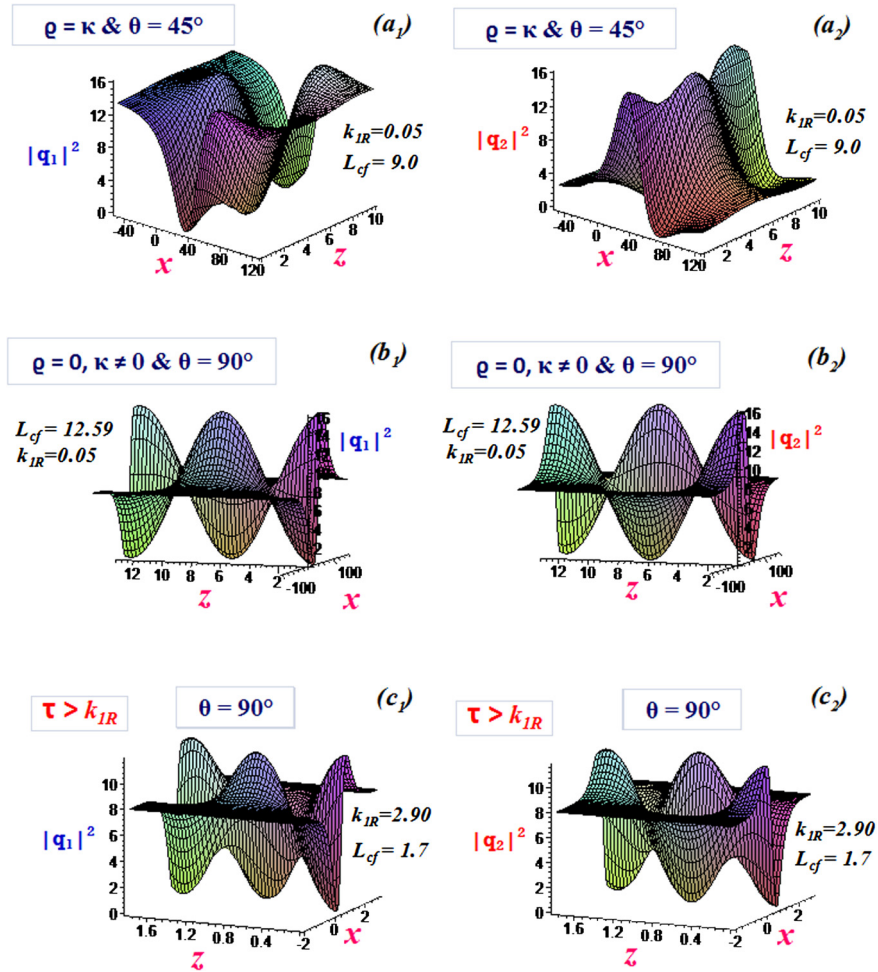
Figure 2. Dynamics of the initial intensity profiles shown in (a) Figure 1(a_2), (b) Figure 1(a_3) and (c) Figure 1(b_1). Note that each breather repeats its initial form periodically at L_{cf}.

(i) the FD–FD vector soliton as shown in Figure 1(b_2), (ii) the amplified scalar dark soliton as shown in Figure 1(b_3), and (iii) the DGB vector soliton as shown in the Figure 1(a_1). If we consider the $d\mu < 0$ case then the breathing effect disappears by forming the B–B vector soliton or the amplified scalar bright soliton or the BGD vector soliton as one expects. Hence if we tune τ and k_{1R} freely without violating the condition $\tau \neq k_{1R}$ while $\theta \neq 0$, then the Eq. (12) supports moving breather vector solitons with different breathing maps within the length L_{cf} as explained below.

If $\tau = 4.0$ and $k_{1R} = 0.05$ (i.e., $\tau \gg k_{1R}$) then for $\theta = 45°$ (i.e., $\kappa = \rho$) and $\theta = 90°$ (i.e., $\rho = 0, \kappa = 0.25$) different breathing maps appear within the $L_{cf} = 9.0$ and $L_{cf} = 12.59$ respectively as shown in Figures 3(a) and 3(b) during the propagation of the initial profiles Figures 1(a_2) and 1(a_3) respectively. The breathing map of the initial profile with $\theta = 90°$ and $k_{1R} = 2.9$ (Figure 1(b_1)) also differs from the previous cases as shown in Figure 3(c). In the Figures 1($a_2, a_3,$
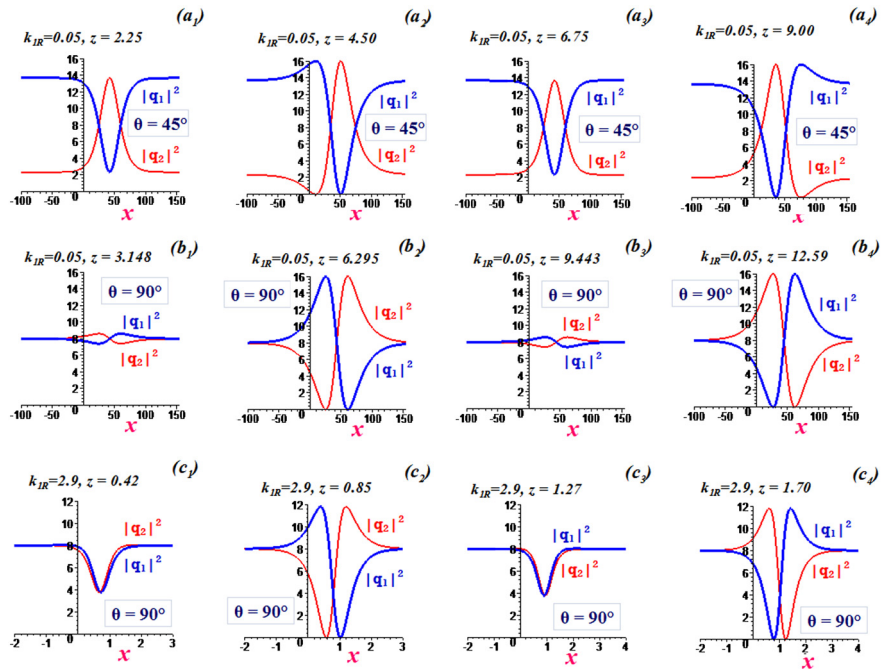
Figure 3. Showing the snapshots of the breather vector soliton dynamics in Figure 2 within the length L_{cf} as (a) Figure 1(a_2), (b) Figure 1(a_3) and (c) Figure 1(b_1), in order to understand different breathing mechanisms associated with the corresponding breathing stills in the Figure 1.

b_1), both q_1 and q_2 are composed with a soliton part and an antisoliton part. Here one component has maximum intensity while other component has zero intensity. In order to understand the breathing mechanism associated with the Figures 1(a_2, a_3, b_1), first we consider the propagation of the initial profile Figure 1(a_3) having equal contribution of soliton and antisoliton parts. During the propagation maximum intensity value of each component decreases uniformly while its minimum intensity value increases. Therefore at one stage the localization parts compress completely. Consequently the components settle at an uniform intensity value against x at $z \approx L_{cf}/4$ (see Figure 3(b_1)). During further propagation the maximum intensity value of each component continuously decreases until the soliton part becomes antisoliton while the minimum intensity value increases until the antisoliton part becomes soliton at $z = L_{cf}/2$ as shown in Figure 3(b_2). Such reversing mechanism here after we refer as pedaling effect. Once again complete compression takes place at $z = 3L_{cf}/4$ as shown in Figure 3(b_3) if one can allow the Figure 1(a_3) to move further. Finally as shown in Figure 3(b_4) at $z = L_{cf} = 12.59$, the initial profile in the Figure 1(a_3) reappears through another pedaling effect. Such breathing map repeats periodically during the propagation as shown in Figure 2(b). Here at every $z \approx nL_{cf}/4$ ($n = 1, 3, 5, ..$) both the breather components not only have uniform intensity value but also stimulate pedaling effect. Hence if $\tau \gg k_{1R}$ and $\theta = 90°$ then the Eq. (12) supports symmetric breather vector soliton. It breathes during the propagation with the help of pedaling mechanism as explained above.

Now we consider the propagation of the initial profile in the Figure $1(b_1)$. In this case the difference between τ and k_{1R} is reduced by increasing the k_{1R} value from 0.05 to 2.9 without affecting the other parametric values. Because of this change the initial profile exhibits different breathing mechanism by composing its form with an unequal combination of antisoliton and soliton parts in its each component as shown in the Figure 3(c). During the propagation the components of such pulse suppress and enhance their localized regions periodically. Consequently during suppression the minimum contribution part (i.e., soliton part of Figure $1(b_1)$) in each component disappears by leaving the excess antisoliton part as a GD–GD vector soliton at $z = L_{cf}/4$ as shown in the breathing map Figure 3(c). During further propagation the localized regions at $L_{cf}/4$ expand into the form as shown in Figure $3(c_2)$ at $L_{cf}/2$. This profile still at $z = L_{cf}/2$ obtained from the initial profile (Figure $1(b_1)$) at $z = 0$ by pedaling its soliton and antisoliton parts of each component into the length of antisoliton and soliton parts. If we permit it to move further GD–GD vector soliton reappears periodically at $z = nL_{cf}/4$ ($n = 1, 3, 5, ..$ as shown in the Figures 2(c) and 3(c) by gradually inhaling the soliton part of each component) and the initial form reappears periodically at $z = nL_{cf}$ ($n = 1, 2, 3, ..$ as shown in Figures 2(c), 3(c) after a complete pedaling).

Next we discuss the breathing mechanism of the initial profile Figure $1(a_2)$ by using the corresponding breathing map in Figure 3(a). Here we set $\theta = 45°$ and $k_{1R} = 0.05$ without affecting the other parametric values in the previous case. Because of such changes, this profile differs from the earlier cases by changing the nature of contribution of a soliton and an antisoliton part. That is, in the q_1 component antisoliton part dominates by permitting very small soliton part while in the q_2 component soliton part dominates by leaving very small part for antisoliton. As in the earlier cases the localized regions of these components gradually compress during the propagation. Consequently the initial profile switched into gray-dark–bright (GD–B) vector soliton at $z = nL_{cf}/4$ ($n = 1, 3, 5, ..$) by compressing the very small localized regions of the components as shown in Figure $3(a_1)$. Further propagation expands the localized regions of the GD–B vector soliton and generates the disappeared parts by toggling the sides of their localized regions. Therefore at each L_{cf} the initial form reappears periodically as shown in Figure 2 by following this breathing map (see Figure 3(a)).

By using the Eq. (11) now we discuss the general case $k_{1I} \neq l$. For this purpose we tune l such that $k_{1I} \sim l$ is small without affecting the other parametric values in the Figure 1. For example if we tune l from 0.25 to 0.23 then the initial profile (FD–B vector soliton with $k_{1I} = l$ in Figure $1(a_1)$ switches into the GD–B vector soliton as shown in Figure $4(a_1)$. If one can introduce the linear cross-coupling effect by tuning θ value then the Figure $4(a_1)$ admits breathing effects as shown in Figures $4(a_2, a_3)$ respectively for $\theta = 45°$ and $\theta = 90°$ while the Figure $1(a_1)$ permits breathing
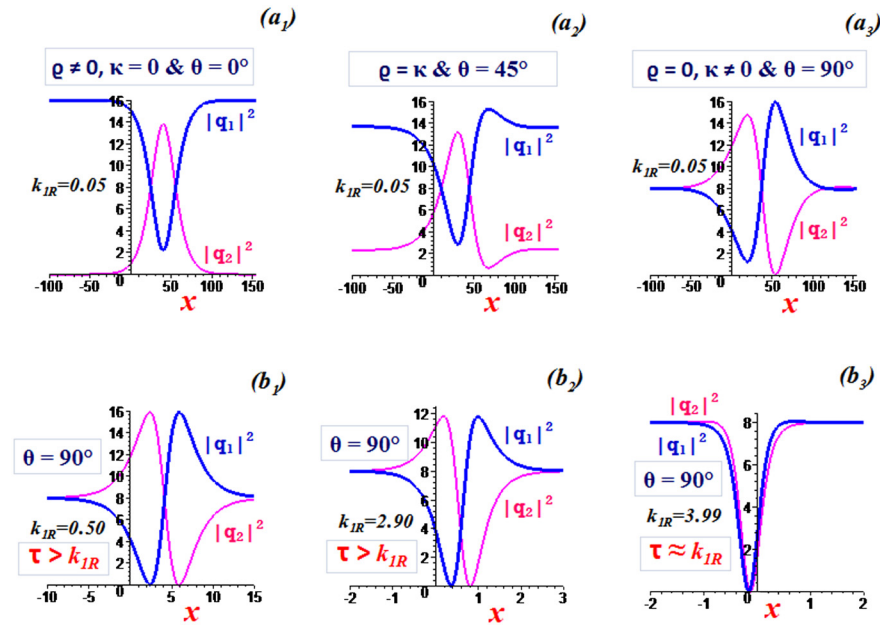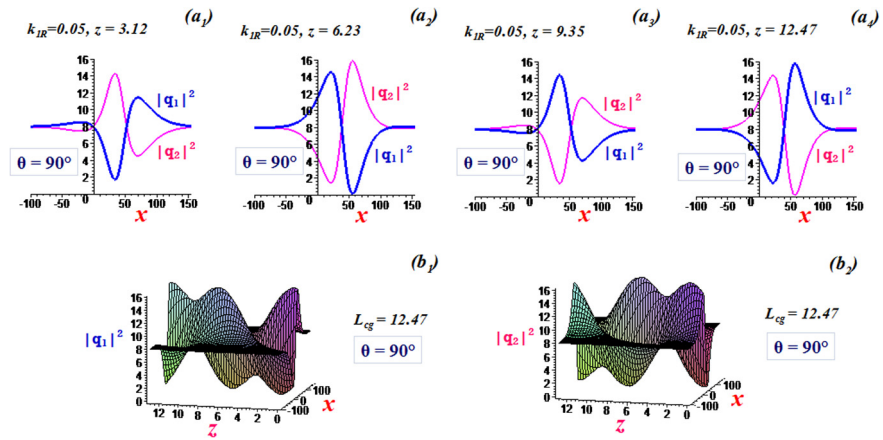
Figure 4. (a_1-a_3) It shows the initial intensity profiles of Eq. (11) under the condition $k_{1I} \simeq l$. Here $k_{1I} = 0.25$, $l = 0.23$ and other parameters are having values as in the Figure 1. By tuning k_{1R} value in the Figure 4(a_3) as shown in (b_1) $k_{1R} = 0.50$, (b_2) $k_{1R} = 2.90$ and (b_3) $k_{1R} = 3.99$.

effect as shown in the Figures 1(a_2, a_3) respectively for $\theta = 45°$ and $\theta = 90°$. It is interesting to note that the Figures 4(a_2, a_3) differ from the Figures 1(a_2, a_3) by changing the ratio of a soliton part and an antisoliton part used to compose them. For example in the Figure 1(a_3) soliton and antisoliton parts equally contribute in each component while in the Figure 4(a_3) such symmetric nature disappears. However in the Figure 4(a_3) one can set such symmetric nature by increasing the k_{1R} value from 0.05 to 0.5 as shown in Figure 4(b_1). It is also interesting to note that the breathing map of Figure 4(a_3) differs from the other cases in the Figure 3 by permitting an additional soliton and antisoliton part while inhaling the localized regions as shown in Figure 5. Hence if $k_{1I} \simeq l$ instead of $k_{1I} = l$ in an initial profile with a breathing effect then some changes appear in the breathing nature as mentioned before. However such changes can be nullified by tuning k_{1R} value or τ value.

What does happen if we tune l such that $k_{1I} \sim l$ is large? In order to answer this question we increase $k_{1I} \sim l$ value from 0.02 to 0.25 by tuning the l value into 0.50 without affecting the other parametric values in the Figure 1. Now the various initial profiles with $\theta \neq 0$ and $\tau \neq k_{1R}$ in the Figure 1 change their breathing vector soliton forms into the multibreather vector soliton forms as shown in Figure 6. It is also interesting to note that the number of soliton and antisoliton parts used to compose q_1 and q_2 components increases as θ increases for given parametric values. However for given θ, it can be controllable as explained below with an example.
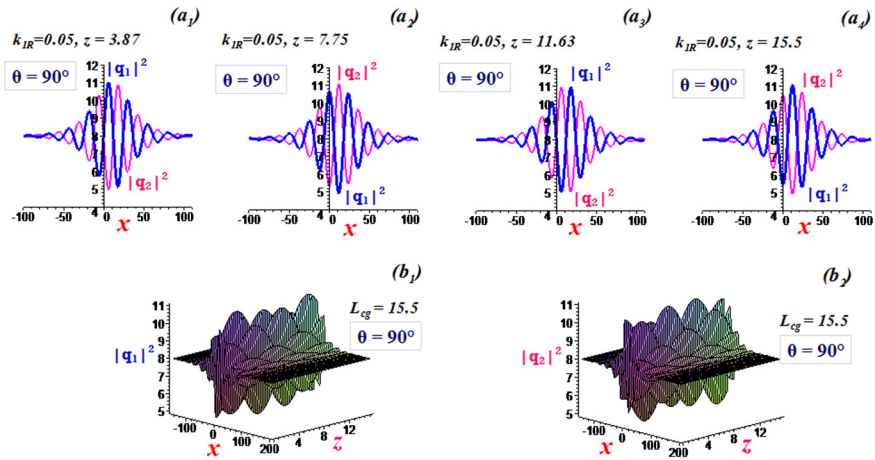
Figure 5. (a_1-a_4) show the snapshots of the dynamics of the Figure 4(a_3). Note that breather repeats its initial form (i.e., Figure 4(a_3)) periodically at L_{cg} as shown in Figure 5b.
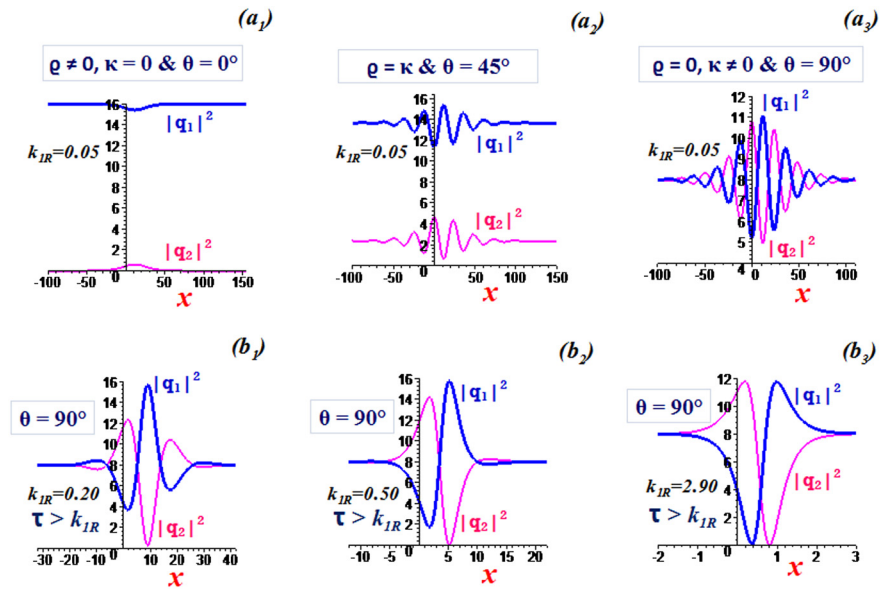
Figure 6. (a_1-a_3) show the initial intensity profiles of Eq. (11) for a given θ value under the condition $l > k_{1I}$. Here we set $l = 0.5$, by keeping the remaining parametric values as in the Figure 4. This case supports multibreather. The multibreathing effect can be suppressed or enhanced by tuning the amplitude parameters τ and k_{1R} suitably as shown in (b_1-b_3).

Consider the initial profile Figure 6(a_3) having complicated form with $\theta = 90°$ and $k_{1R} = 0.05$. It repeats its form periodically at $L_{cg} = 15.5$ (as dictated by the Eq. (13)) during the propagation as shown in the Figure 7(b) with a breathing map Figure 7(a). The more number of soliton and antisoliton parts in each component of this case can be reduced with a breathing effect by increasing the k_{1R} value towards τ value such that $|\tau|^2 cos^2 \varphi \neq \frac{d}{\mu} k_{1R}^2$ as shown in the Figure 6.

Figure 7. $(a_1 - a_4)$ illustrate the snapshots of the multibreather vector soliton dynamics in the Figure $6(a_3)$. Note that breather repeats its initial form (i.e., Figure $6(a_3)$) periodically at L_{cg} as shown in Figure 7b.

3.2. Modified Manakov model under the influence of linear terms and multibreather vector solitons

Now we consider the modified Manakov equation ($\sigma = -1$) with the linear coupling terms [49] as

$$
iq_{1_z} + dq_{1_{xx}} + \rho q_1 - \kappa q_2 - 2\mu(|q_1|^2 - |q_2|^2)q_1 = 0,
$$
$$
iq_{2_z} + dq_{2_{xx}} - \rho q_2 + \kappa q_1 - 2\mu(|q_1|^2 - |q_2|^2)q_2 = 0. \tag{15}
$$

The above Eq. (15) reduces to the modified Manakov equation (5) under the transformation with hyperbolic function as

$$
q_1 = \cosh(\theta/2)e^{i\Gamma z}q_{1_M} + \sinh(\theta/2)e^{-i\Gamma z}q_{2_M},
$$
$$
q_2 = \sinh(\theta/2)e^{i\Gamma z}q_{1_M} + \cosh(\theta/2)e^{-i\Gamma z}q_{2_M}, \tag{16}
$$

where $\theta = \tanh^{-1}(\kappa/\rho)$ and $\Gamma = \sqrt{\rho^2 - \kappa^2}, \kappa \leq \rho$. The nature of transformation varies from the earlier case because of the changes in the signs of σ and linear cross coupling coefficients. When $\kappa = 0$, then the Eq. (15) reduced to the Lindner–Fedyanin system [42] which is a one-dimensional continuum limit of two dimensional (2D) Hubbard model. In addition, we trust that such mathematical model can be used to study the left handed materials and also be introduced in the BECs that induces Rabi oscillation or Josephson oscillation between the population of two states [50].

As in the previous section, by substituting the BD vector soliton solution of the Eq. (5) in the Eq. (16), one can obtain the equations for the intensity profiles of one-soliton solution of the Eq. (15) as

$$
|q_1|^2 = \cosh^2(\theta/2)|\tau|^2 \sin^2\varphi + \cosh^2(\theta/2)|\tau|^2 \cos^2\varphi \tanh^2(\eta_{1R} + \frac{\xi}{2})
$$

$$+ \sinh^2(\theta/2)(\frac{d}{\mu}k_{1R}^2 - |\tau|^2 \cos^2 \varphi) \sec h^2(\eta_{1R} + \frac{\xi}{2}) + \sinh\theta|\tau|$$

$$\sqrt{\frac{d}{\mu}k_{1R}^2 - |\tau|^2 \cos^2 \varphi} \sec h(\eta_{1R} + \frac{\xi}{2}) \sin\varphi \sin(\psi_1 + \varphi + \zeta - \eta_{1I} + 2\Gamma z)$$

$$- \sinh\theta|\tau|\sqrt{\frac{d}{\mu}k_{1R}^2 - |\tau|^2 \cos^2 \varphi} \sec h(\eta_{1R} + \frac{\xi}{2}) \cos\varphi \tanh(\eta_{1R} + \frac{\xi}{2})$$

$$\cos(\psi_1 + \varphi + \zeta - \eta_{1I} + 2\Gamma z),$$

$$|q_2|^2 = \sinh^2(\theta/2)|\tau|^2 \sin^2 \varphi + \sinh^2(\theta/2)|\tau|^2 \cos^2 \varphi \tanh^2(\eta_{1R} + \frac{\xi}{2})$$

$$+ \cosh^2(\theta/2)(\frac{d}{\mu}k_{1R}^2 - |\tau|^2 \cos^2 \varphi) \sec h^2(\eta_{1R} + \frac{\xi}{2}) + \sinh\theta|\tau|$$

$$\sqrt{\frac{d}{\mu}k_{1R}^2 - |\tau|^2 \cos^2 \varphi} \sec h(\eta_{1R} + \frac{\xi}{2}) \sin\varphi \sin(\psi_1 + \varphi + \zeta - \eta_{1I} + 2\Gamma z)$$

$$- \sinh\theta|\tau|\sqrt{\frac{d}{\mu}k_{1R}^2 - |\tau|^2 \cos^2 \varphi} \sec h(\eta_{1R} + \frac{\xi}{2}) \cos\varphi \tanh(\eta_{1R} + \frac{\xi}{2})$$

$$\cos(\psi_1 + \varphi + \zeta - \eta_{1I} + 2\Gamma z). \tag{17}$$

As mentioned before the above equation is valid only in the region $d\mu > 0$. Moreover as it supports the hyperbolic functions instead of the circular functions in the transformation equation, the role of θ differs from the earlier case. The value of θ (i.e., the role of ρ and κ) defines the amount of contribution of the first two terms in the Eq. (17) and the influence of oscillating terms. For example if $\theta = 0°$ (i.e., $\rho = 1$ and $\kappa = 0$), $|q_1|^2$ and $|q_2|^2$ are the intensity profiles of bright–dark. For other θ values first two terms of Eq. (17) are never equally contribute due to the presence of hyperbolic functions in the transformation equation (16). Therefore it is interesting to note from Figure 8 that the q_1 supports soliton/antisoliton part while q_2 also supports soliton/antisoliton part. However the contribution of each part never becomes symmetric and hence avoiding the possibility of appearing pedaling effect in the breathing maps. This modified case also supports periodically varying breathing vector solitons with different breathing maps due to the presence of oscillating terms. Moreover here breathing mechanism is not same under certain parametric choices as in the earlier case.

For example in the $\theta = 90°$ case if $\tau \rightarrow k_{1R}$ we get dark–dark vector soliton by suppressing breathing effect as shown in Figure 8(b_3). Because here $q_{2M} = 0$ as $\tau \rightarrow k_{1R}$. Therefore the resultant solution is valid in the SDF region. On the other hand, if $\tau \rightarrow 0$ (i.e., $q_{1M} \rightarrow 0$) then the BB vector soliton appears in the SF region as shown in Figure 8(b_1) by suppressing the breathing effects otherwise as shown in Figure 8(b_2). Moreover at $\theta = 0°$ it supports bright–dark intensity profile as shown in Figure 8(a_1). If we increase the value of θ the initial intensity varies as shown in the Figures 8(a_2–a_3). During the propagation such initial pulses vary periodically by following certain breathing maps.
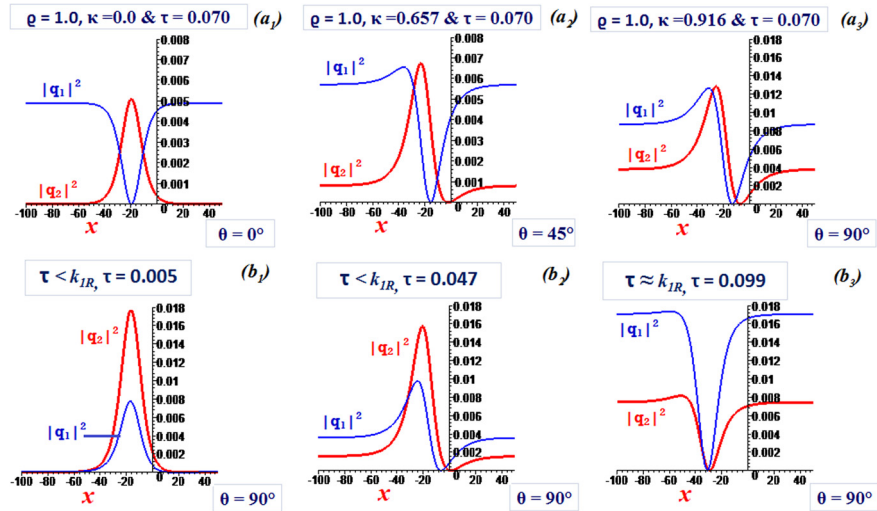
Figure 8. (a_1-a_3) show the initial intensity profiles of Eq. (17) under the parametric choices $k_{1I} = l = 0.025$, $k_{1R} = 0.1$ and $d = \mu = 0.5$. In this case an initial breathing profile can be switched into BB or DD or another breathing form by tuning the amplitude parameters k_{1R} and τ appropriately as shown in (b_1-b_3).

3.3. Multibreather two-soliton with different collision scenarios

In order to study the interaction effects between two such periodically varying breather vector one-solitons, first we have derived the vector multibreather two-soliton of Eq. (8) by using the mixed vector two-soliton solution of the Manakov model [11] in the transformation (9) as

$$q_1 = \cos(\theta/2)e^{i\Gamma z}\frac{\psi^{(1)}}{D} - \sin(\theta/2)e^{-i\Gamma z}\frac{\psi^{(2)}}{D},$$

$$q_2 = \sin(\theta/2)e^{i\Gamma z}\frac{\psi^{(1)}}{D} + \cos(\theta/2)e^{-i\Gamma z}\frac{\psi^{(2)}}{D}, \tag{18}$$

where $\psi^{(1)} = \tau e^{(i\psi_1)}(1 - \sum_{j,k=1}^{2}\frac{\rho_j}{\rho_k^*}\mu_{jk}e^{\eta_j+\eta_k^*} + \chi^{(1)})$, $\psi^{(2)} = \sum_{j=1}^{2}e^{\eta_j} + \sum_{j=1}^{2}\nu_{12}\mu_{1j}\mu_{2j}e^{\eta_1+\eta_j^*+\eta_2}$, $D = 1 + \sum_{j,k=1}^{2}\mu_{jk}e^{\eta_j+\eta_k^*} + Fe^{\eta_1+\eta_1^*+\eta_2+\eta_2^*}$, $\nu_{jk} = -(k_j - k_k)^2\left[\frac{|\tau|^2}{\rho_j\rho_k} + \frac{d}{\mu}\right]$, $\chi^{(1)} = \frac{\rho_1\rho_2}{\rho_1^*\rho_2^*}Fe^{\eta_1+\eta_1^*+\eta_2+\eta_2^*}$, $\mu_{jk} = \left[(k_j + k_k^*)^2\left(\frac{|\tau|^2}{\rho_j\rho_k^*} - \frac{d}{\mu}\right)\right]^{-1}$, $F = \mu_{11}\mu_{22}|\mu_{12}\nu_{12}|^2$, $\eta_{jR} = k_{jR}x - 2dk_{jR}k_{jI}z + \eta_{jR}^{(0)}$, $\eta_{jI} = k_{jI}x + (d(k_{jR}^2 - k_{jI}^2) - \lambda)z + \eta_{jI}^{(0)}$, $\eta_j^{(0)} = \eta_{jR}^{(0)} + i\eta_{jI}^{(0)}$, $k_j = k_{jR} + ik_{jI}$, $\rho_j = k_j - il$ for $(j = 1, 2)$.

The asymptotic analysis reveals us that Eq. (18) defines two well separated multibreather vector one-solitons appearing before and after collisions respectively at the limits $z \to +\infty$ and $z \to -\infty$. These two-solitons at $z \to \pm\infty$ take the form (9) with different parameters for pulse-width (k_{jR}) and velocity (k_{jI}) but with the same background field for the dark components in each colliding vector one-soliton.
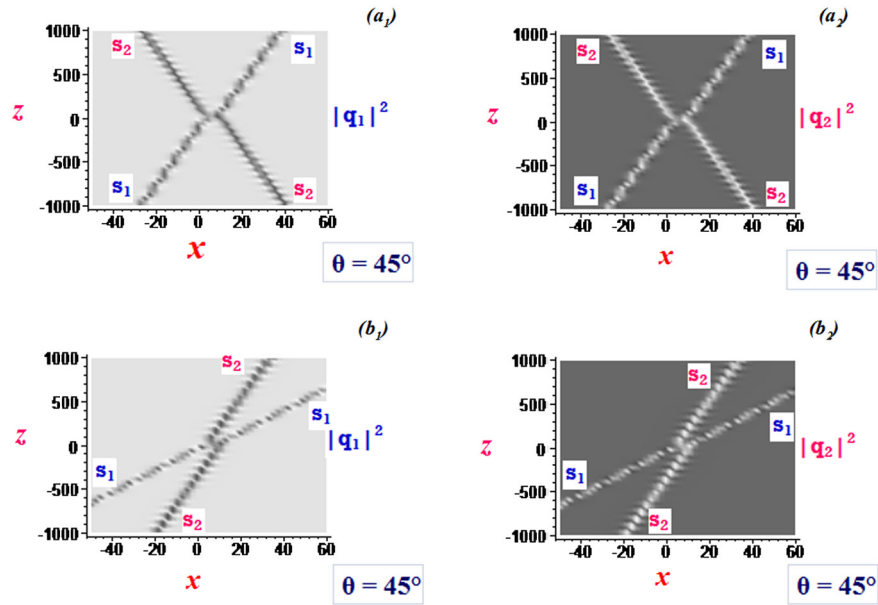
Figure 9. Smooth collision dynamics of Eq. (18) under the parametric choices $\tau = 4.0$, $k_{1R} = 0.75$, $k_{2R} = 0.57$, $l = 0.06$, $d = \mu = 0.5$ (a) $k_{2I} = -k_{1I} = 0.03$ and (b) $k_{1I} = 0.08$ and $k_{2I} = 0.03$.

The collision does not affect any soliton parameters other than the phase-constant. Therefore our aim is to study the interaction effects between two such solitons with different velocities when they are packed closely by tuning the pulse-width parameters k_{jR} appropriately. As one expects collision dynamics of Eq. (18) appears as a head on collision as shown in Figure 9(a) if the sign of velocity parameter k_{1I} and that of k_{2I} are different. Otherwise it looks like an overtaking collision as shown in Figure 9(b). Here other parameters don't restrict the nature of appearance of collision dynamics. In the Figure 9 the collision is very smooth without any effects in the SDF colliding region. By taking the case corresponding to Figure 9(a) different interaction effects can be found in the colliding region by tuning pulse-width and velocity parameters as discussed below.

If we decrease the k_{1R} value from 0.75 to 0.55, k_{2R} value from 0.57 to 0.37 and $|k_{jI}|$ value from 0.03 to 0.01, then the beating effect (i.e., components of colliding solitons beat each other in the colliding region) introduced in the Figure 9(a) as shown in Figure 10(a). Without affecting the velocity parameters in the Figure 9(a), if we decrease the value of k_{1R} from 0.75 to 0.55 and k_{2R} from 0.57 to 0.50, then the jumping effect introduced in the colliding region of Figure 9(a) as shown in Figure 10(b). All these cases (corresponding to the Figures 9, 10) are having attractive collisions with the different interaction effects in the colliding regions. Is it able to change the nature of such collision? Yes, it is possible to change the nature of collision as a reflective collision. As an example in the Figure 9(a), we have introduced the reflection effect by setting $\triangle k_R = 0.02$ as shown in Figure 11(a). In this case one can introduce the beating effect by increasing the velocity value
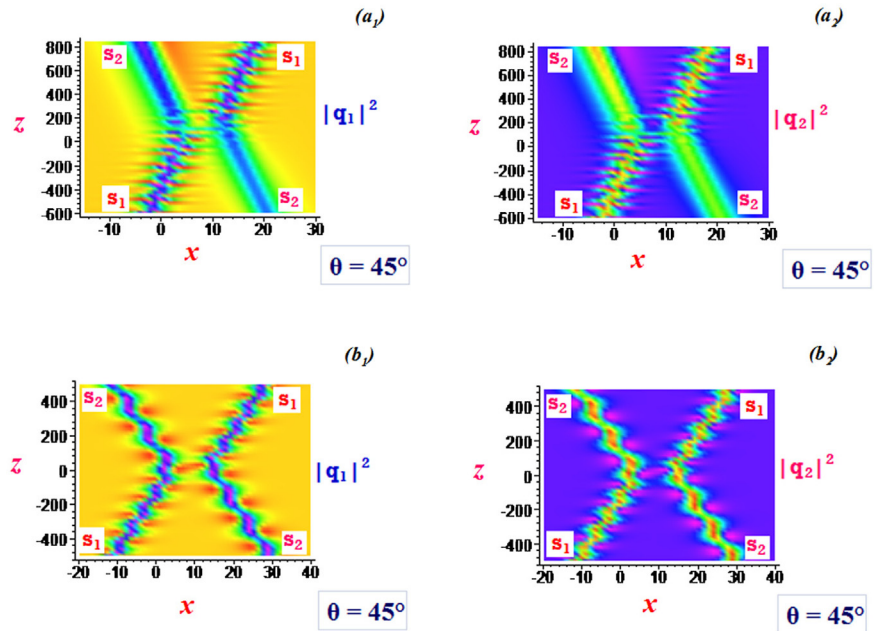
Figure 10. Attractive collision dynamics with (a) beating effect, (b) jumping effect.
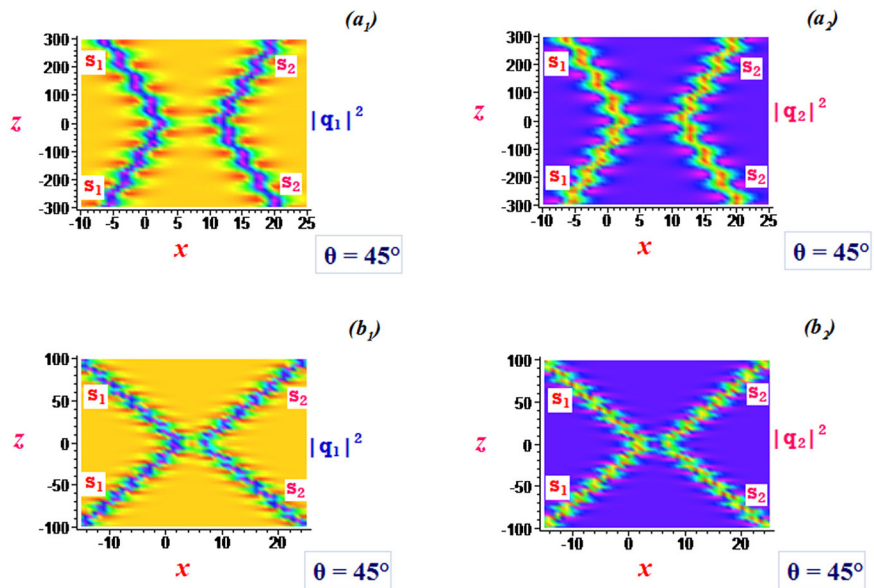

Figure 11. Collision dynamics with (a) reflection effect, (b) beating effect.

from 0.03 to 0.15 as shown in Figure 11(b). If we closely pack two solitons with same velocity by taking $k_{1R} = 0.77$, $k_{2R} = 0.70$ and $k_{1I} = k_{2I} = 0.00$, then an additional breathing effect appears in the Figure 9(a) due to the effects of one on the other as shown in Figure 12(a). This effect disappears if we increase the initial separation distance as shown in Figure 12(b). Finally by selecting the suitable parametric values it is also possible to study the collision dynamics between breather
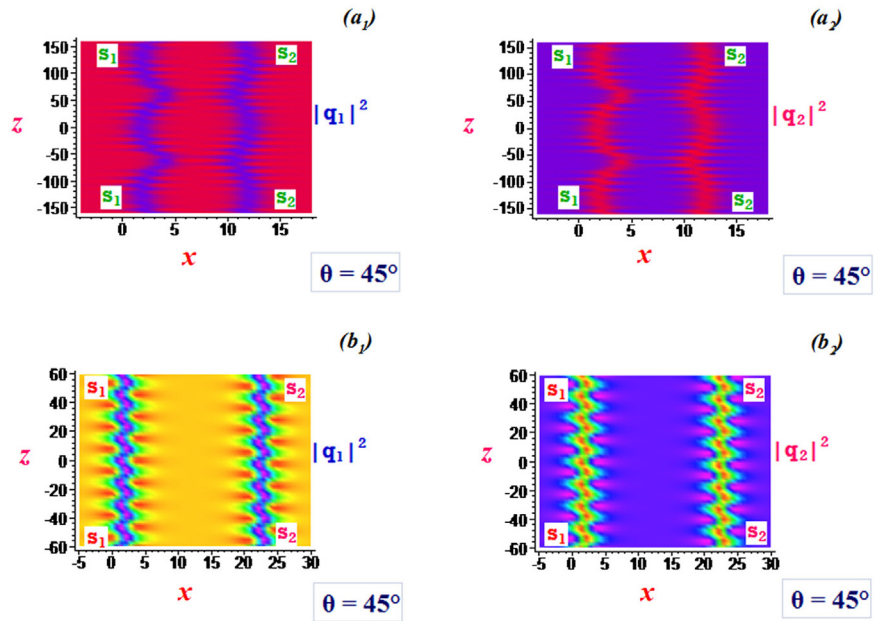
Figure 12. (a) Interaction effect between the two closely packed breather vector one-solitons with same velocities. (b) Suppressing such interaction effect by decreasing the $\triangle k_R$ value in order to increase the initial separation distance.

vector one-solitons with different breathing maps. As an example, in Figure 13(a) we have numerically demonstrated the collision dynamics between simple breather and complicated multibreather vector one-solitons under the parametric choices $\tau = 4.0$, $k_{1R} = 0.55$, $k_{1I} = -0.01$, $k_{2R} = 0.37$, $k_{2I} = 0.02$, $l = 0.70$ and $d = \mu = 0.5$. We have also demonstrated the collision dynamics between the two complicated multibreather vector one-solitons as shown in Figure 13(b) under the parametric choices $\tau = 4.0$, $k_{1R} = 0.60$, $k_{1I} = 0.02$, $k_{2R} = 0.4$, $k_{2I} = -0.02$, $l = 0.20$ and $d = \mu = 0.5$. Moreover the collision dynamics between two breather vector one-soliton solutions of the modified CNLS equation (15) with the negative nonlinear cross-coupling can also be investigated by using the two-soliton solutions of the modified Manakov model [35, 49].

4. Conclusions

In conclusion, it is interesting to reveal that the DGB vector soliton of the Manakov model [11] exists in the parametric domain $\frac{|\tau|^2}{|p_1|^2} > \frac{d}{\mu}$ of the SDF region while its BGD vector soliton appears freely in the SF region. If we change the sign of the XPM, the resulting solution is a BD vector soliton in the parametric domain $\frac{d}{\mu} > \frac{|\tau|^2}{|p_1|^2}$ of the SDF region. We have also defined the changes in these solutions due to the changes in the signs of d and μ. By influencing all such physically interesting solutions with the effects corresponding to the terms proportional to κ and ρ one
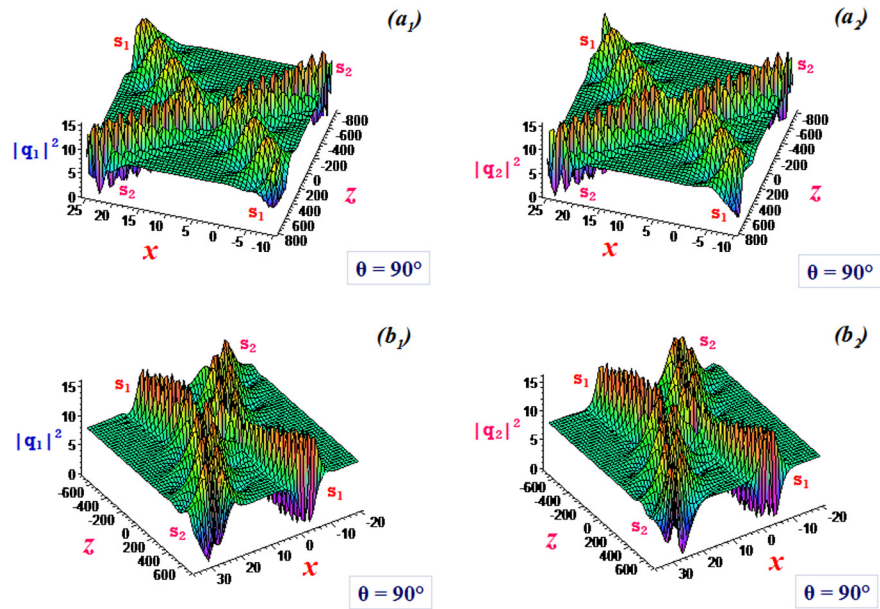
Figure 13. (a) Collision between symmetric breather and multibreather. (b) Collision between multibreathers.

can generate multibreather vector soliton. Such soliton in this paper has freedom to control the number of soliton and antisoliton parts used to compose it. Moreover its breathing mechanism (or) breathing map and breathing length are tunable. One can switch this breathing mechanism from one kind to other kind. Moreover by suppressing the breathing effect one can generate the DD or BB or BD vector soliton or the amplified scalar soliton as shown in the Figures 1, 4 and 8. Moreover different interaction effects in between them are realized. Such effects can be suppressed or enhanced by using the soliton parameters. Because of such features we believe that this kind of study will further give impetus on the Lindner–Fedyanin system in the continuum limit, and find the potential applications in fiber coupler and also in BECs. Further the Manakov model and its modified forms with the coupling terms used for our studies are receiving continuous interest in the literature [42, 43, 44, 45, 46, 47, 48, 49] due to their various potential applications as mentioned in the section 3. The effects of loss and other possible XPM values, etc. [48, 52, 53] can also be investigated in somewhere else by using the obtained solution as an unperturbed part [33].

Declarations

Author contribution statement

Nagarajan Manikandan, Rengarj Radhakrishnan: Conceived and designed the analysis; Analyzed and interpreted the data; Wrote the paper.

Funding statement

Competing interest statement

The authors declare no conflict of interest.

Additional information

No additional information is available for this paper.

References

[1] Yu S. Kivshar, B.L. Davies, Dark optical solitons: physics and applications, Phys. Rep. 298 (1998) 81.

[2] Yu S. Kivshar, G.P. Agrawal, Optical Solitons, Academic Press, San Diego, 2003.

[3] N.N. Akhmediev, A. Ankiewicz, Solitons Nonlinear Pulses and Beams, Chapman and Hall, London, 1997.

[4] C.R. Menyuk, Nonlinear pulse propagation in birefringent optical fibers, IEEE J. Quantum Electron. 23 (1987) 174–176.

[5] C.R. Menyuk, Pulse propagation in an elliptically birefringent Kerr medium, IEEE J. Quantum Electron. 25 (1989) 2674–2682.

[6] S.V. Manakov, On the theory of two-dimensional stationary self-focusing of electromagnetic waves, Zh. Èksp. Teor. Fiz. 65 (1973) 505–516; Sov. Phys. JETP 38 (1974) 248.

[7] V.E. Zakharov, A.B.Shabat, Exact theory of two-dimensional self-focusing and one-dimensional self-modulation of waves in nonlinear media, Zh. Eksp. Teor. Fiz. 61 (118) (1971); Sov. Phys. JETP 34 (1972) 62–69.

[8] V.E. Zakharov, A.B. Shabat, Interaction between solitons in a stable medium, Zh. Eksp. Teor. Fiz. 64 (1973) 1627; Sov. Phys. JETP 37 (1973) 823–828.

[9] N. Bélanger, A. Villeneuve, J.S. Aitchison, Soliton like pulses in self-defocusing AlGaAs waveguides, J. Opt. Soc. Am. B 14 (1997) 3003–3012.

[10] R. Radhakrishnan, M. Lakshmanan, Bright and dark soliton solutions to coupled nonlinear Schrödinger equations, J. Phys. A, Math. Gen. 28 (1995) 2683–2692.

[11] A.P. Sheppard, Y.S. Kivshar, Polarized dark solitons in isotropic Kerr media, Phys. Rev. E 55 (1997) 4773–4782.

[12] R. Radhakrishnan, K. Aravinthan, A dark–bright optical soliton solution to the coupled nonlinear Schrödinger equation, J. Phys. A, Math. Theor. 40 (2007) 13023–13030.

[13] R. Radhakrishnan, K. Aravinthan, Spatial vector soliton and its collisions in isotropic self-defocusing Kerr media, Phys. Rev. E 75 (2007) 066605.

[14] R. Radhakrishnan, M. Lakshmanan, J. Hietarinta, Inelastic collision and switching of coupled bright solitons in optical fibers, Phys. Rev. E 56 (1997) 2213–2216.

[15] R. Radhakrishnan, P.T. Dinda, G. Millot, Efficient control of the energy exchange due to the Manakov vector-soliton collision, Phys. Rev. E 69 (2004) 046607.

[16] M.H. Jakubowski, K. Steiglitz, R. Squier, State transformations of colliding optical solitons and possible application to computation in bulk media, Phys. Rev. E 58 (1998) 6752–6758.

[17] K. Steiglitz, Time-gated Manakov spatial solitons are computationally universal, Phys. Rev. E 63 (2000) 016608.

[18] K. Steiglitz, Multistable collision cycles of Manakov spatial solitons, Phys. Rev. E 63 (2001) 046607.

[19] C. Anastassiou, J.W. Fleischer, T. Carmon, M. Segev, K. Steiglitz, Information transfer via cascaded collisions of vector solitons, Opt. Lett. 26 (2001) 1498–1500.

[20] C. Anastassiou, M. Segev, K. Steiglitz, J.A. Giordmaine, M. Mitchell, M. Shih, S. Lan, J. Martin, Energy-exchange interactions between colliding vector solitons, Phys. Rev. Lett. 83 (1999) 2332–2335.

[21] A.A. Sukhorukov, N.N. Akhmediev, Multiport soliton devices with controllable transmission, Opt. Lett. 28 (2003) 908–910.

[22] N. Lazarides, G.P. Tsironis, Coupled nonlinear Schrödinger field equations for electromagnetic wave propagation in nonlinear left-handed materials, Phys. Rev. E 71 (2005) 036614.

[23] J. Babarro, M.J. Paz-Alonso, H. Michinel, J.R. Salgueiro, D.N. Olivier, Controllable scattering of vector Bose–Einstein solitons, Phys. Rev. A 71 (2005) 043608.

[24] B.G. Vahala, L. Vahala, J. Yepez, Inelastic vector soliton collisions: a lattice-based quantum representation, Philos. Trans. R. Soc. Lond. A 362 (2004) 1677–1690.

[25] D. Rand, I. Glesk, C.S. Brés, D.A. Nolan, X. Chen, J. Koh, J.W. Fleischer, K. Steiglitz, P.R. Prucnal, Observation of temporal vector soliton propagation and collision in birefringent fiber, Phys. Rev. Lett. 98 (2007) 053902.

[26] K. Aravinthan, Exact Multicomponent Vector Optical Solitons in Nonlinear Kerr Media, PhD thesis, 2009. Submitted to the Bharathidasan University, India.

[27] V.E. Zakharov, E.I. Schulman, To the integrability of the system of the two coupled nonlinear Schrödinger equations, Physica D 4 (1982) 270–274.

[28] V.G. Makhankov, N.N. Makhaldiani, O.K. Pashaev, On the integrability and isotopic structure of the one-dimensional Hubbard model in the long wave approximation, Phys. Lett. A 81 (1981) 161–164.

[29] R. Radhakrishnan, R. Sahadevan, M. Lakshmanan, Integrability and singularity structure of coupled nonlinear Schrödinger equations, Chaos Solitons Fractals 5 (1995) 2315–2327.

[30] E.N. Tsoy, N. Nail Akhmediev, Dynamics and interaction of pulses in the modified Manakov model, Opt. Commun. 266 (2006) 660–668.

[31] Y. Ohta, D.S. Wang, J. Yang, General N-dark–dark solitons in the coupled nonlinear Schrödinger equations, Stud. Appl. Math. 127 (2011) 345–371.

[32] D.S. Wang, D. Zhang, J. Yang, Integrable properties of the general coupled nonlinear Schrödinger equations, J. Math. Phys. 51 (2010) 023510.

[33] P.T. Dinda, R. Radhakrishnan, T. Kanna, Energy-exchange collision of the Manakov vector solitons under strong environmental perturbations, J. Opt. Soc. Am. B 24 (2007) 592–605.

[34] T. Kanna, M. Lakshmanan, P.T. Dinda, N. Akhmediev, Soliton collisions with shape change by intensity redistribution in mixed coupled nonlinear Schrödinger equations, Phys. Rev. E 73 (2006) 026604.

[35] R. Radhakrishnan, Exact Coupled Optical Solitons in Fibers, PhD thesis, 1997. Submitted to the Bharathidasan University, India.

[36] M. Vijayajayanthi, T. Kanna, M. Lakshmanan, Bright–dark solitons and their collisions in mixed N-coupled nonlinear Schrödinger equations, Phys. Rev. A 77 (2008) 013820.

[37] N. Manikandan, R. Radhakrishnan, K. Aravinthan, Generalized dark–bright vector soliton solution to the mixed coupled nonlinear Schrödinger equations, Phys. Rev. E 90 (2014) 022902.

[38] S. Inouye, J. Goldwin, M.L. Olsen, C. Ticknor, J.L. Bohn, D.S. Jin, Observation of heteronuclear Feshbach resonances in a mixture of bosons and fermions, Phys. Rev. Lett. 93 (2004) 183201.

[39] C.A. Stan, M.W. Zwierlein, C.H. Schunck, S.M.F. Raupach, W. Ketterle, Observation of Feshbach resonances between two different atomic species, Phys. Rev. Lett. 93 (2004) 143001.

[40] I. Bloch, M. Greiner, O. Mandel, T.W. Hänsch, T. Esslinger, Sympathetic cooling of ^{85}Rb and ^{87}Rb, Phys. Rev. A 64 (2001), 021402(R).

[41] A.G. Kalocsai, J.W. Haus, Asymptotic wave–wave processes beyond cascading in quadratic nonlinear optical materials, Phys. Rev. E 52 (1995) 3166–3183.

[42] U. Lindner, V. Fedyanin, Solitons in a one-dimensional modified Hubbard model, Phys. Status Solidi B 89 (1978) 123–129.

[43] C. Elphick, The quantum spectral transform method for the one- and two-component nonlinear Schrödinger model, J. Phys. A, Math. Gen. 16 (1983) 4013–4024.

[44] P.A. Bélanger, C. Paré, Soliton switching and energy coupling in two-mode fibers: analytical results, Phys. Rev. A 41 (1990) 5254–5256.

[45] M.J. Potasek, Soliton solution for coupled periodically twisted birefringent optical fibers, J. Opt. Soc. Am. B 10 (1993) 941–945.

[46] R. Radhakrishnan, M. Lakshmanan, Suppression and enhancement of soliton switching during interaction in periodically twisted birefringent fiber, Phys. Rev. E 60 (1999) 2317.

[47] G. Kakarantzas, A.O. Blanch, T.A. Birks, P.S.J. Russell, L. Farr, F. Couny, B.J. Mangan, Structural rocking filters in highly birefringent photonic crystal fiber, Opt. Lett. 28 (2003) 158–160.

[48] G.P. Agrawal, Nonlinear Fiber Optics, 2nd ed., Academic Press, New York, 1995.

[49] T. Kanna, M. Vijayajayanthi, M. Lakshmanan, Periodic energy switching of bright solitons in mixed coupled nonlinear Schrödinger equations with linear self-coupling and cross-coupling terms, Phys. Rev. A 76 (2007) 013808.

[50] B. Xiong, Localized asymmetric atomic matter waves in two-component Bose–Einstein condensates coupled with two photon microwave field, arXiv:nlin/0703001v1 [nlin.PS], 2007.

[51] V.G. Makhankov, O.K. Pashaev, Nonlinear Schrödinger equation with non compact isogroup, Teor. Mat. Fiz. 53 (1982) 55–67.

[52] S. Trillo, S. Wabnitz, W.C. Banyai, N. Finlayson, C.T. Seaton, G.I. Stegeman, R.H. Stolen, Observation of ultrafast nonlinear polarization switching induced by polarization instability in a birefingent fiber rocking filter, IEEE J. Quantum Electron. 25 (1989) 104–112.

[53] S. Wabnitz, S. Trillo, E.M. Wright, G.I. Stegman, Wavelength-dependent soliton self-routing in birefringent fiber filters, J. Opt. Soc. Am. B 8 (1991) 602–613.